International Journal of Thermophysics, Vol. 16, No. 5, 1995

Effects of Weak Shear on Hyperswollen Lyotropic Smectic Liquid Crystals[1]

J. Yamamoto[2,3] and H. Tanaka[2]

We have developed a Zimm-type viscometer specially designed for the simultaneous measurements of the structure factor and the viscosity of hyperswollen lyotropic liquid crystals under a very weak shear. We have investigated the shear effects on the layer undulation fluctuation in the lamellar structure and the transition from the anisotropic lamellar to the isotropic sponge phase. We have found a significant difference in the rheological properties between the lamellar and the sponge phase: The former exhibits non-Newtonian flow behavior, while the latter exhibits Newtonian behavior.

KEY WORDS: liquid crystal; rheology; shear effects; viscometer.

1. INTRODUCTION

Complex fluids exhibit unique rheological properties, reflecting their soft structure organized by a weak, but long-range interaction. Recently, much attention has been paid to the mechanical properties of complex fluids such as liquid crystals [1–3], polymer solutions [4–6], and colloidal crystals. The shear effects on the phase stability and the structural fluctuation are particularly interesting since these complex fluids have many internal degree of freedom which are directly coupled with the velocity fields, and thus their structures can be very sensitive even to a very weak shear field.

Among the various types of complex fluids, the hyperswollen lyotropic smectic phase [7, 8] is unique in the sense that it has an anisotropic

[1] Paper presented at the Twelfth Symposium on Thermophysical Properties, June 19–24, 1994, Boulder, Colorado, U.S.A.

[2] Institute of Industrial Science, University of Tokyo, Minato-ku, Tokyo 106, Japan.

[3] To whom correspondence should be addressed.

0195-928X/95/0900-1099$07.50/0

structure. In the lyotropic smectic phase, the infinite bilayers and water layers are alternatively stacked. Thus it has the same symmetry (one-dimensional order) as the usual thermotropic smectic A phase. For the lyotropic smectic phase, however, thermally excited undulation fluctuations of the membrane strongly affect the physical nature of this phase. Further, the lyotropic smectic phase is composed of two components—membranes and intermembrane fluid layers—and thus we must consider this phase on the basis of the two-fluid model. These facts cause the essential differences between the lyotropic and the thermotropic smectic phases. Since the neighboring membranes sterically hinder the undulation fluctuation, this loss of conformational entropy leads to a so-called steric interaction [9]. This entropic intermembrane interaction is much more long-range than the usual interactions such as van der Waals and the hydration forces. Thus the lyotropic smectie phase made of the soft membranes is stable even in a very dilute region, where the interlamellar repeat distance is comparable to the wavelength of the visible light [8]: Surprisingly, the lattice constant of the one-dimensional positional order can be thousands of angstroms.

To investigate the shear effects on such a dilute complex fluid in a very weak shear regime, we have developed a Zimm-type viscometer, which allows us to perform simultaneous measurements of structural and theological properties. The scattering function (Bragg peak) under a steady shear flow has been successfully measured by sweeping the wavelength of light. Here we briefly report the shear effects on both the hyperswollen lamellar phase and the sponge phase in a weak shear regime.

2. METHODS

Since our major interest is the shear effects on the structure and its fluctuation, we need to study the structure of lyotropic liquid crystals under a shear field. For this purpose, we developed a new Zimm-type viscometer. In addition to its ability for simultaneous measurements of theological and structural properties, this system has several characteristics which are suitable for studying the weakly interacting system. The most important feature is that the applied stress is very low (0.005–0.2 $dyn \cdot cm^{-2}$), which allows us to study the response of the system for a weak perturbation. Further, since our viscometer consists of coaxial double cylinders, a uniform shear flow field can be achieved, in contrast to the case of a capillary viscometer, which has a Poiseuille's flow field. Our viscometer is also suitable for checking whether a finite yield stress exists, because we can measure the stress–strain relationship from an extremely small shear rate. Furthermore, the monodomain sample can be easily obtained since the shear flow aligns the smectic layers along the flow direction. The

preparation of a monodomain sample which has an almost-perfect alignment is a prerequisite for the detailed shape analysis of the scattering function under shear.

2.1. Zimm-Type Viscometer

The structure of the viscometer shown schematically in Fig. 1. The viscometer consists of three main parts: a freely floating inner cylinder (rotor), an outer large cylinder (stator), and a permanent magnet rotating around the cylinder. The stator is fixed on the base and is in contact with the temperature-controlled water bath around it. The temperature stability of the sample is ~ 0.05 K. The rotor floats on the sample in the stator by its buoyancy. The total mass of the rotor must be adjusted to be balanced with its buoyant force so that the rotor is fully submerged in the sample as shown in Fig. 1. The rotor axis is spontaneously located on the cylindrical axis of the stator due to the surface tension acting on the edge of the rotor. Thus we achieve a coaxial double-cylinder configuration with a uniform gap. The inside radius of the stator R_0 and the outside radius of the rotor R_i, are 10 and 9 mm, respectively. The gap between the rotor and the stator is 1 mm.

Here we describe the principle of our Zimm-type viscometer, which is essentially the same as that described by Mitaku et al. [10]. The rotation of the permanent magnet by the pulse motor causes a rotating torque T_m on an aluminum cylinder which is fixed to the rotor, through the interaction between the rotating magnetic field and the induced magnetic

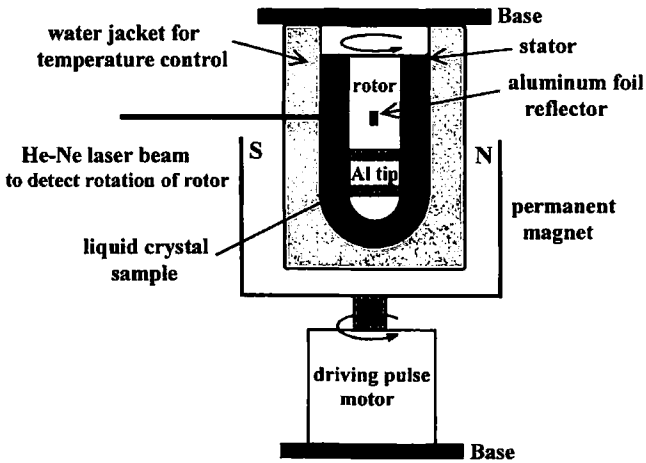

Fig. 1. Schematic diagram of the Zimm-type viscometer.

moment. Thus the rotor is forced to turn. This magnetically induced torque T_m is given by

$$T_m = \alpha(\omega_m - \omega_r) \tag{1}$$

where ω_m and ω_r are the angular velocity of the rotating magnetic field and the rotor, respectively. In the steady state, this torque should be balanced with the viscous frictional torque T_v, which is caused by the velocity gradient in the sample sandwiched between the stator and the rotor. This torque is related to the viscosity η and ω_r as

$$T_v = \beta\eta\omega_r \tag{2}$$

where the prefactor β is dependent only on the geometry of the rotor and the stator. From the relation $T_m = T_v$ we obtain

$$\alpha(\omega_m - \omega_r) = \beta\eta\omega_r \tag{3}$$

On the other hand, the average shear rate $\langle\dot{\gamma}\rangle$ is given by

$$\langle\dot{\gamma}\rangle = \frac{4R_o^2R_i^2}{(R_o^2 - R_i^2)^2} \ln\left(\frac{R_o}{R_i}\right)\omega_r = A_\gamma\omega_r \tag{4}$$

This prefactor A_γ is obviously dependent only on the geometry of the stator and the rotor. The torque balance equation yields, for the average shear stress $\langle\sigma\rangle$,

$$\langle\sigma\rangle = \eta\langle\dot{\gamma}\rangle = \frac{\alpha}{\beta}A_\gamma(\omega_m - \omega_r) = A_\sigma(\omega_m - \omega_r) \tag{5}$$

$$A_\sigma = \frac{\alpha}{\beta}A_\gamma \tag{6}$$

To obtain the relationship between the shear stress and the shear rate, we need to measure ω_r as a function of ω_m. Then the shear rate $\dot{\gamma}$ is directly obtained from ω_r by Eq. (4). The shear stress σ is also obtained with the aid of Eq. (5). We used pure water as a viscosity standard to determine A_σ, because its viscosity is almost the same as that of the sample and its temperature dependence is well-known. Non-Newtonian flow behavior is obtained from the shear-rate dependence of the viscosity. For the precise measurement of ω_r, a small reflector made of aluminum foil is put on the side of the rotor as indicated in Fig. 1. The reflected light of a He–Ne laser is monitored with a photodetector to measure the period of rotation.

2.2. Static Light Scattering

Since most of the Zimm-type viscometer is made of glass, we can shine light into the sample under a shear flow. To study one-dimensional positional ordering, the light scattering measurement is performed under shear flow. Instead of the usual static lightscattering configuration of scanning the scattering angle, we sweep the wavelength of the incident light. The Xe-lamp light was filtered by a monochromator to obtain monochromatic incident light. The wavelength of the incident light was limited to the range from 370 to 700 nm, by both the transparency of the glass cell and the ability of the monochromator. The wavelength resolution was 0.5 nm. Two lenses and a slit were used to attain a parallel incident light beam. To observe the one-dimensional order of the smectic phase, the scattering geometry was chosen as indicated in Fig. 2, so that the scattering vector is normal to the layers. It is desired that the scattering angle 2θ is fixed near 180°, since if θ (which is equal to the angle between layers and the incident light, see Fig. 2) is much different from 90°, it is hard to make the scattering vector coincide with the layer normal within the scattering volume, because of the finite curvature of the glass wall of the cell. However, θ cannot be exactly equal to 90° because of the harmful effect of stray light reflected by the outside glass surface of the stator. Since the glass wall has finite curvature, the stray light and the signal light beam do not overlap with each other as indicated in Fig. 2, for $\theta \neq 90°$. In our experiments, therefore, θ was fixed to 85°, and the stray light was cut by putting the slit

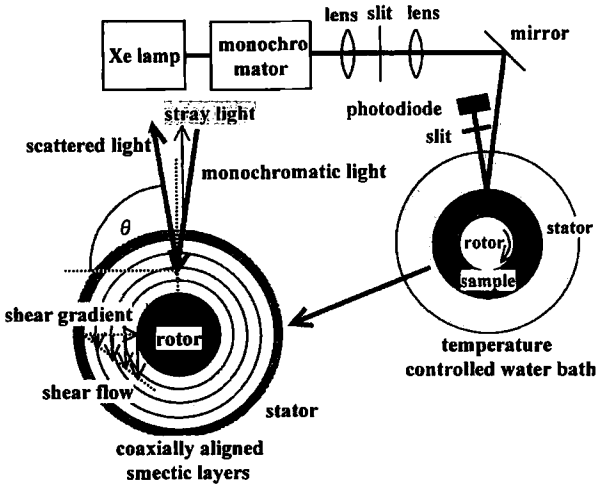

Fig. 2. Block diagram of the system for measuring the static light-scattering sweeping the wavelength of the incident light.

just in front of the photodiode. This limitation on θ is the main reason why we adopt the wavelength-sweeping method instead of the angle-scanning method. This was possible because the characteristic length scale of the hyperswollen lamellar phase is comparable to the wavelength of visible light and thus a nearly backscattering configuration can be used.

The wavelength of the incident light was almost continuously swept by the pulse motor, which rotated the grating in the monochromator. The scattered light intensity was then recorded in a microcomputer through an A/D converter. The dependence of the incident light intensity on the wavelength coming from the spectrum of the Xe lamp was corrected after the measurements. Thus the scattering function of the smectic liquid crystals around the Bragg peak was successfully observed under a weak steady shear field.

3. EXPERIMENTS

We have studied aqueous solutions of pentaethyleneglycol dodecyl ether ($C_{12}E_5$; Nikko Chemicals BL5SY). This system has various types of liquid crystalline phases, dependent on the temperature and surfactant concentration [8]. Among these phases, we focused our attention on the lamellar phase (L_α) and the sponge phase (L_3) (see Fig. 3). The former is an anisotropic smectic phase, while the latter is an isotropic phase. The L_3 phase appears at higher temperatures than the L_α phase. In the L_3 phase, the membranes are randomly interconnected. The samples mainly studied here were dilute solutions of $C_{12}E_5$ ($\leqslant 2.0$ wt%).

Since the solution is phase-separated at room temperature, it must be stirred for a while in the viscometer in the one-phase L_α region to attain

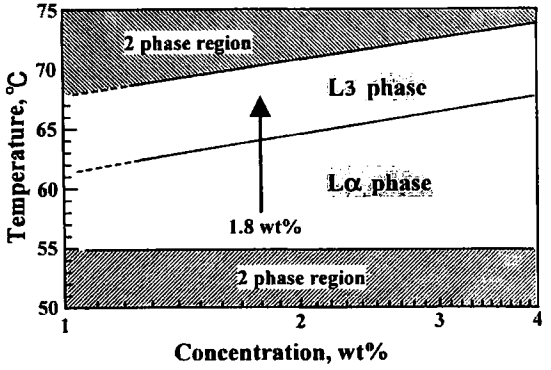

Fig. 3. Schematic phase diagram of a $C_{12}E_5$/water mixture in the dilute region.

the homogeneous L_α phase. The homeotropic alignment of the lamellar phase in the viscometer is confirmed by the fact that the solution is uniformly colored.

4. RESULTS AND DISCUSSIONS

Figure 4 shows the typical wavenumber dependence of the scattered light intensity as a function of the applied shear stress for the solution of 1.80 wt% $C_{12}E_5$ at 60.1°C. The Bragg peak is clearly observed irrespective of the existence of the shear flow. The peak wavelength gives the lamellar repeat distance and its width provides us with the information on the large fluctuations which are characteristic of such a one-dimensional system. The Bragg peak is shifted toward the shorter wavelength and becomes broader with an increase in the shear stress. The physical origin of this behavior will be discussed in detail elsewhere [11]. These results clearly indicate the applicability of the Zimm-type viscometer modified for the structural study.

Figure 5 shows the dependence of the viscosity on the shear stress at several temperatures for both the L_α and the L_3 phases. In the L_α phase, the viscosity is strongly dependent on the shear stress; namely, non-Newtonian flow behavior is observed. The L_3 phase, on the other hand, exhibits the usual Newtonian flow behavior, but the viscosity is a few times higher than that of L_α phase. The shear-rate dependence of viscosity in the L_α phase becomes weaker with approaching the L_α–L_3 phase transition. The flow behavior appears to be Newtonian even in the vicinity of the L_α–L_3 phase transition. It should also be noted that we observe no yield stress for either phase.

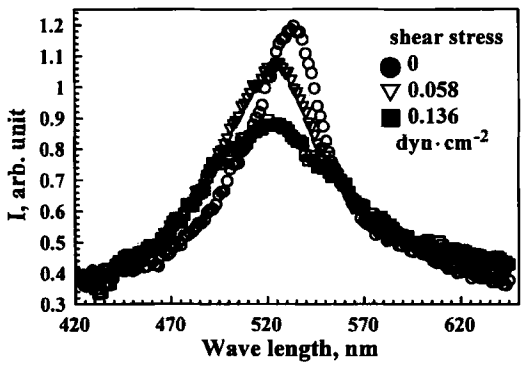

Fig. 4. Wavenumber dependence of the Bragg scattering intensity as a function of the shear stress ($C_{12}E_5$, 1.80 wt%, 60.1°C).

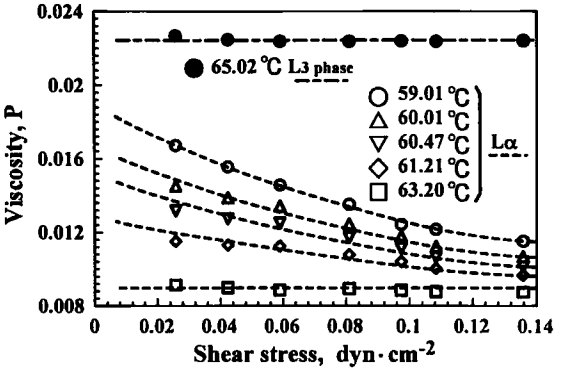

Fig. 5. Dependence of the viscosity on the shear stress for the L_α and L_3 phases. The lines are a guide for the eye.

5. SUMMARY

We have constructed an improved Zimm-type viscometer and demonstrated that this system is very useful for investigating the shear effects on the structure and its fluctuation of a complex fluid having many internal degrees of freedom. Simultaneous measurements of rheological and structural properties are a prerequisite for understanding the shear effects on such a complex fluid on a microscopic level. We hope that the complicated couplings between the velocity field and the fluctuation modes in complex fluids will be clarified by this sort of study in the near-future.

ACKNOWLEDGMENT

This work was partly supported by a Grant-in-Aid from the Ministry of Education, Culture, and Science, Japan.

REFERENCES

1. O. Diat, D. Roux, and F. Nallet, *J. Phys. II France* **3**:1427 (1993).
2. D. Roux, F. Nallet, and O. Diat, *Europhys. Lett.* **24**:53 (1993).
3. R. Bruinsma and Y. Rabin, *Phys. Rev. A* **45**:994 (1992).
4. M. Doi and A. Onuki, *J. Phys II (France)* **2**:1631 (1992); and references therein.
5. H. Tanaka, *Phys. Rev. Lett.* **71**:3158 (1993); *J. Chem. Phys.* **100**:5323 (1994).
6. S. T. Milner, *Phys. Rev. E* **48**:3674 (1993).

7. C. R. Safinya, D. Roux, G. S. Smith, S. K. Sinha, P. Dimon, N. A. Clark, and A. M. Bellocq, *Phys. Rev. Lett.* **57**:2718 (1986); D. Roux and C. R. Safinya, *J. Phys. France* **49**:307 (1988).
8. R. Strey, R. Schomacker, D. Roux, F. Nallet, and U. Olsson, *J. Chem. Soc. Faraday Trans.* **86**:2253 (1990).
9. W. Helfrich, *Z. Naturforsch* **33a**:305 (1978).
10. S. Mitaku, T. Ohtuki, and K. Okano, *J. Phys. France* **40**:C3-481 (1979).
11. J. Yamamoto and H. Tanaka, unpublished.